Time-resolved fluorescence line-narrowing of Eu^{3+} in biocompatible eutectic glass-ceramics

D. Sola,[1] R. Balda,[1,2,*] M. Al-Saleh,[2] J. I. Peña,[3] and J. Fernández[1,2]

[1]*Materials Physics Center CSIC-UPV/EHU and Donostia International Physics Center, 20080 San Sebastián, Spain*
[2]*Departamento de Física Aplicada I, Escuela Técnica Superior de Ingeniería, Universidad del Pais Vasco UPV/EHU, Alda. Urquijo s/n 48013 Bilbao, Spain*
[3]*Instituto de Ciencia de Materiales de Aragón, Universidad de Zaragoza-CSIC, 50018 Zaragoza, Spain*
**wupbacrr@bi.ehu.es*

Abstract: The spectroscopic properties of Eu^{3+} in biocompatible glass and glass-ceramic eutectic rods of composition $0.8CaSiO_3$-$0.2Ca_3(PO_4)_2$ doped with 0.5 wt% of Eu_2O_3 are investigated to explore their potential applications as optical probes. The samples were obtained by the laser floating zone technique. Depending on the growth rate, they exhibit three (two crystalline and one amorphous) or two (one crystalline and one amorphous) phases. The crystalline phases correspond to Ca_2SiO_4 and apatite-like structures. At high growth rates the system presents an amorphous arrangement which gives a glass phase. The results of time-resolved fluorescence line narrowing spectroscopy obtained under excitation within the inhomogeneous broadened $^7F_0 \rightarrow {}^5D_0$ absorption band allow to isolate the emission from Eu^{3+} ions in the crystalline and amorphous environments and to accurately correlate the spectroscopic properties with the microstructure of these eutectics.

OCIS codes: (160.5690) Rare-earth-doped materials; (300.6320) Spectroscopy, high-resolution; (160.1435) Biomaterials.

References and links

1. L. L. Hench, R. J. Splinter, T. K. Greenle, and W. C. Allen, "Bonding mechanisms at the interface of ceramic prosthetic materials," J. Biomed. Mater. Res. **2**, 117–141 (1971).
2. L. L. Hench, "Bioceramics: From Concept to Clinic," J. Am. Ceram. Soc. **74**(7), 1487–1510 (1991).
3. K. De Groot and R. Le Geros, *Significance of Porosity and Physical Chemistry of Calcium Phosphate Ceramics*, P. Ducheyne, ed. (Ann. N.Y. Acad. Sci.,1988).
4. P. N. de Aza, F. Guitian, and S. de Aza, "Phase diagram of wollastonite-tricalcium phosphate," J. Am. Ceram. Soc. **78**(6), 1653–1656 (1995).
5. P. N. De Aza, F. Guitián, and S. De Aza, "Bioeutectic: a new ceramic material for human bone replacement," Biomaterials **18**(19), 1285–1291 (1997).
6. M. Magallanes-Perdomo, A. H. De Aza, I. Sobrados, J. Sanz, and P. Pena, "Structure and properties of bioactive eutectic glasses based on the $Ca_3(PO_4)_2$-$CaSiO_3$-$CaMg(SiO_3)_2$ system," Acta Biomater. **8**(2), 820–829 (2012).
7. J. Llorca and V. M. Orera, "Directionally solidified eutectic ceramic oxides," Prog. Mater. Sci. **51**(6), 711–809 (2006).
8. R. I. Merino, J. A. Pardo, J. I. Peña, G. F. de la Fuente, A. Larrea, and V. M. Orera, "Luminescence properties of ZrO_2-CaO eutectic crystals with ordered lamellar microstructure activated with Er^{3+} ions," Phys. Rev. B **56**(17), 10907–10915 (1997).
9. V. M. Orera, J. I. Peña, R. I. Merino, J. A. Lazaro, J. A. Valles, and M. A. Rebolledo, "Prospects of new planar optical waveguides based on eutectic microcomposites of insulating crystals: The ZrO_2(c)-$CaZrO_3$ erbium doped system," Appl. Phys. Lett. **71**(19), 2746–2748 (1997).
10. R. G. Carrodeguas and S. De Aza, "α-Tricalcium phosphate: Synthesis, properties and biomedical applications," Acta Biomater. **7**(10), 3536–3546 (2011).
11. P. N. de Aza, F. Guitian, and S. de Aza, "A new bioactive material which transforms *in situ* into hydroxyapatite," Acta Mater. **46**(7), 2541–2549 (1998).
12. M. Magallanes-Perdomo, P. Pena, P. N. De Aza, R. G. Carrodeguas, M. A. Rodríguez, X. Turrillas, S. De Aza, and A. H. De Aza, "Devitrification studies of wollastonite-tricalcium phosphate eutectic glass," Acta Biomater. **5**(8), 3057–3066 (2009).
13. J. A. Pardo, J. I. Peña, R. I. Merino, R. Cases, A. Larrea, and V. M. Orera, "Spectroscopic properties of Er^{3+} and Nd^{3+} doped glasses with $0.8CaSiO_3$-$0.2Ca_3(PO_4)_2$ eutectic composition," J. Non-Cryst. Solids **298**(1), 23–31 (2002).

#181528 - $15.00 USD Received 10 Dec 2012; revised 26 Feb 2013; accepted 1 Mar 2013; published 8 Mar 2013

14. R. Balda, J. Fernández, I. Iparraguirre, J. Azkargorta, S. García-Revilla, J. I. Peña, R. I. Merino, and V. M. Orera, "Broadband laser tunability of Nd^{3+} ions in $0.8CaSiO_3$-$0.2Ca_3(PO_4)_2$ eutectic glass," Opt. Express **17**(6), 4382–4387 (2009).
15. R. Balda, R. I. Merino, J. I. Peña, V. M. Orera, and J. Fernández, "Laser spectroscopy of Nd^{3+} ions in glasses with the $0.8CaSiO_3$–$0.2Ca_3(PO_4)_2$ eutectic composition," Opt. Mater. **31**(9), 1319–1322 (2009).
16. D. Sola, R. Balda, J. I. Peña, and J. Fernández, "Site-selective laser spectroscopy of Nd^{3+} ions in $0.8CaSiO_3$-$0.2Ca_3(PO_4)_2$ biocompatible eutectic glass-ceramics," Opt. Express **20**(10), 10701–10711 (2012).
17. R. Balda, J. Fernández, J. L. Adam, and M. A. Arriandiaga, "Time-resolved fluorescence-line narrowing and energy-transfer studies in a Eu^{3+}-doped fluorophosphates glass," Phys. Rev. B **54**(17), 12076–12086 (1996).
18. C. Cascales, J. Fernández, and R. Balda, "Investigation of site-selective symmetries of Eu^{3+} ions in KPb_2Cl_5 by using optical spectroscopy," Opt. Express **13**(6), 2141–2152 (2005).
19. C. Cascales, R. Balda, V. Jubera, J. P. Chaminade, and J. Fernández, "Optical spectroscopic study of Eu^{3+} crystal field sites in $Na_3La_9O_3(BO_3)_8$ crystal," Opt. Express **16**(4), 2653–2662 (2008).
20. H. Nagabhushana, B. M. Nagabhushana, M. Madesh Kumar, K. V. R. Chikkahanumantharayappa, K. V. R. Murthy, C. Shivakumara, and R. P. S. Chakradhar, "Synthesis, characterization and photoluminescence properties of $CaSiO_3$: Eu^{3+} red phosphor," Spectrochimica Acta Part A **78**(1), 64–69 (2011).
21. X. Kang, S. Huang, P. Yang, P. Ma, D. Yang, and J. Lin, "Preparation of luminescent and mesoporous Eu^{3+}/Tb^{3+} doped calcium silicate microspheres as drug carriers via a template route," Dalton Trans. **40**(9), 1873–1879 (2011).
22. S. J. Dhoble, N. S. Dhoble, and R. B. Pode, "Preparation and characterization of Eu^{3+} activated $CaSiO_3$, $(CaA)SiO_3$ [A = Ba or Sr] phosphors," Bull. Mater. Sci. **26**(4), 377–382 (2003).
23. Y. Fan, S. Huang, J. Jiang, G. Li, P. Yang, H. Lian, Z. Cheng, and J. Lin, "Luminescent, mesoporous, and bioactive europium-doped calcium silicate (MCS: Eu^{3+}) as a drug carrier," J. Colloid Interface Sci. **357**(2), 280–285 (2011).
24. Q. Yu, Y. Liu, S. Wu, X. Lü, X. Huang, and X. Li, "Luminescence properties of Ca_2SiO_4:Eu^{3+} red phosphor for trichromatic white light emitting diodes," J. Rare Earths **26**(6), 783–786 (2008).
25. A. Doat, M. Fanjul, F. Pellé, E. Hollande, and A. Lebugle, "Europium-doped bioapatite: a new photostable biological probe, internalizable by human cells," Biomaterials **24**(19), 3365–3371 (2003).
26. X. H. Chuaia, H. J. Zhang, F. Sh. Li, Sh. Z. Lu, J. Lin, Sh. B. Wang, and K. Chi-Chou, "Synthesis and luminescence properties of oxyapatite $NaY_9Si_6O_{26}$ doped with Eu^{3+}, Tb^{3+}, Dy^{3+} and Pb^{2+}," J. Alloy. Comp. **334**, 211–218 (2002).
27. M. Karbowiak and S. Hubert, "Site-selective emission spectra of Eu^{3+}:$Ca_5(PO_4)_3F$," J. Alloy. Comp. **302**(1-2), 87–93 (2000).
28. B. Piriou, D. Fahmi, J. Dexpert-Ghys, A. Taitai, and J. L. Lacout, "Unusual fluorescent properties of Eu^{3+} in oxyapatites," J. Lumin. **39**(2), 97–103 (1987).
29. K. Madhukumar, H. K. Varma, M. Komath, T. S. Elias, V. Padmanabhan, and C. M. K. Nair, "Photoluminescence and thermoluminescence properties of tricalcium phosphate phosphors doped with dysprosium and europium," Bull. Mater. Sci. **30**(5), 527–534 (2007).
30. W. Xue, S. Zhai, and H. Zheng, "Synthesis and photoluminescence properties of Eu^{3+}-doped γ-$Ca_3(PO_4)_2$," Mater. Chem. Phys. **133**(1), 324–327 (2012).
31. D. Sola, F. J. Ester, P. B. Oliete, and J. I. Peña, "Study of the stability of the molten zone and the stresses induced during the growth of Al_2O_3–$Y_3Al_5O_{12}$ eutectic composite by the laser floating zone technique," J. Eur. Ceram. Soc. **31**(7), 1211–1218 (2011).
32. F. J. Ester, D. Sola, and J. I. Peña, "Thermal stresses in the Al_2O_3-ZrO_2 (Y_2O_3) eutectic composite during the growth by the laser floating zone technique," Bol. Soc. Esp. Ceram. **47**, 352–357 (2008).
33. F. J. Ester and J. I. Peña, "Analysis of the molten zone in the growth of the Al_2O_3-ZrO_2 (Y_2O_3) eutectic by the laser floating zone technique," Bol. Soc. Esp. Ceram. **46**, 240–246 (2007).
34. A. Oyane, H. M. Kim, T. Furuya, T. Kokubo, T. Miyazaki, and T. Nakamura, "Preparation and assessment of revised simulated body fluids," J. Biomed. Mater. Res. A **65A**(2), 188–195 (2003).
35. Z. Gou, J. Chang, and W. Zhai, "Preparation and characterization of novel bioactive dicalcium silicate ceramics," J. Eur. Ceram. Soc. **25**(9), 1507–1514 (2005).

1. Introduction

Ceramic biomaterials study for tissue repair and bone replacement has been developed throughout the last decades since the discovery of a bioactive glass by Hench et al. in 1970 [1]. A common characteristic of these materials is the formation of a hydroxyapatite (HA) layer on their surface when soaked into simulated body fluid (SBF) [2]. Equally, when bioactive ceramic materials are implanted in a living body the interaction between the bone and these materials also takes place only on their surface. To improve the ingrowth of new bone into the implant, the use of materials with an appropriate interconnected porous structure is recommended [3]. An approach to overcome this problem is to use dense bioactive materials capable of developing porous structures *in situ* after being implanted. To fulfil this purpose the material should be constituted by at least two phases, bioactive and resorbable,

#181528 - $15.00 USD Received 10 Dec 2012; revised 26 Feb 2013; accepted 1 Mar 2013; published 8 Mar 2013

respectively. Suitable candidates for this purpose are eutectic glasses and glass-ceramics of the CaO-SiO_2-P_2O_5 and CaO-SiO_2-P_2O_5-MgO systems [4–6].

Directionally solidified eutectics are composite materials grown from the melt by means of a controlled system. They have shown more relevant properties than their crystalline counterparts with the same composition due to the unique microstructures that can be created during the solidification process. The characteristics of this complex and homogeneous microstructure which can be controlled by the solidification conditions have provided them with excellent mechanical properties, microstructural stability and corrosion resistance up to temperatures very close to their melting point [7]. In addition to their excellent performance as structural materials, the unique features of the eutectic microstructure allow extending the use of these materials to functional applications by the addition of rare earths (RE) to the eutectic system. For instance, the contrast in the refractive index between the constituent phases allows to produce efficient light guiding in some eutectic ceramics [8, 9].

The eutectic wollastonite (W)-tricalcium phosphate (TCP) binary system has been widely studied throughout the last decades since it belongs to the family of bioceramic materials. In particular, tricalcium phosphate, $Ca_3(PO_4)_2$, is osteoconductive and bioactive (resorbable) whereas wollastonite, $CaSiO_3$, is bioactive with osteostimulative properties [4, 5, 10–12]. Worth mentioning is the fact that this material presents a high reactivity in simulated body fluid (SBF) so that when soaked into SBF an alteration of the material, based on the solution of W into SBF and a pseudomorphic transformation of TCP into HA is produced, giving rise to a thin layer of porous material. In addition, this eutectic glass, when doped with rare earths, has shown excellent optical properties [13–15].

Recent results have shown that the transformation of this eutectic glass-ceramics doped with Nd^{3+} ions when soaked into SBF could be analyzed in vitro by using rare-earth ions as luminescence probes. Site-selective laser spectroscopy in the $^4I_{9/2}\rightarrow{}^4F_{3/2}/^4F_{5/2}$ transitions of Nd^{3+} ions were used to investigate the crystal field changes felt by Nd^{3+} ions as a consequence of the sample crystallization stage. The differences among the spectral features of the site-selective excitation and emission spectra of Nd^{3+} ions allowed discerning between crystalline and amorphous environments for the rare-earth ions as well as to attempt correlating the spectroscopic properties with the microstructure of these eutectic materials [16]. However, due to the complexity of the Nd^{3+} ion levels and to the spectral overlapping of the emissions coming from the rare earth ion in different amorphous and crystalline environments, it was impossible to isolate the emission corresponding to individual crystalline phases. With the aim of clearly identifying the rare-earth emission from the amorphous and crystalline phases in these eutectics, Eu^{3+} ions which are highly sensitive to the local environment, have been used as probe ions in this work. Since $^5D_0$ state is non-degenerate under any symmetry, the structure of the $^5D_0\rightarrow{}^7F_J$ emission is only determined by the splitting of the terminal levels caused by the local crystal field. Moreover, as the $^7F_0$ level is also non-degenerate, site-selective excitation within the $^7F_0\rightarrow{}^5D_0$ absorption band can be performed by using fluorescence line narrowing (FLN) spectroscopy in order to distinguish among different local environments around the Eu^{3+} ions [17–19].

The work investigates the microstructural and photoluminescence properties of the binary system $CaSiO_3$-$Ca_3(PO_4)_2$ in the eutectic composition doped with Eu^{3+} ions as a function of the crystallization stage of the host matrix. Although photoluminescence properties have been studied in calcium silicate [20–23], dicalcium silicate [24], apatite-like structure [25–28], and tricalcium phosphate phosphors [29, 30], most of these works deal with low spectral resolved luminescence of Eu^{3+} obtained under non-selective UV excitation to explore its intense red emission for applications in phosphor materials [20, 22, 24, 29, 30] and drug release tracking [21, 23, 25]. Site-selective emission spectra of Eu^{3+}-doped fluoroapatite and oxyapatite structures are reported in Refs. 27 and 28 where the presence of different crystal field sites for Eu^{3+} ions depending on the method of preparation are identified. In this work, and for the first time to our knowledge, time-resolved fluorescence line narrowing (TRFLN) spectroscopy of Eu^{3+} in the eutectic glassy as well as glass-ceramic stages are reported. For this purpose, the samples were fabricated by the laser floating zone technique (LFZ) which permits to obtain

#181528 - $15.00 USD Received 10 Dec 2012; revised 26 Feb 2013; accepted 1 Mar 2013; published 8 Mar 2013

shaped fiber glasses and glass-ceramic materials up to 4 mm in diameter. Furthermore, it allows controlling the solidification rate by means of the growth rate, providing high axial and radial thermal gradients in the liquid-solid interface [7, 31–33], of paramount importance in the final microstructure obtained, in such a way that glasses and glass-ceramic materials can be produced. The spectroscopic properties of Eu^{3+} in biocompatible glass and glass-ceramic eutectic rods of composition $0.8CaSiO_3$-$0.2Ca_3(PO_4)_2$ doped with 0.5 wt% of Eu_2O_3 are investigated to explore their potential applications as optical probes and identify the different micro-structural phases present in the glass ceramic. The samples were obtained by the laser floating zone technique at different growth rates between 50 and 1000 mm/h. The microstructural analysis shows the existence of three (two crystalline and one amorphous) or two phases (one crystalline and one amorphous) depending on the growth rate. The crystalline phases correspond to Ca_2SiO_4 and apatite-like structures. At high growth rates the system presents an amorphous arrangement which gives a glass phase. The Ca_2SiO_4 crystalline structure observed in the glass-ceramic samples grown at low rate shows high reactivity when soaked into simulated body fluid giving rise to a porous layer.

The results of fluorescence line narrowing experiments demonstrate the existence of three different local environments around the Eu^{3+} ions in these eutectic samples. The line structure in the TRFLN spectra together with the remarkably different lifetime values of the $^5D_0$ state as a function of excitation wavelength allows to isolate the emission from Eu^{3+} ions in the crystalline and amorphous environments and to accurately correlate the spectroscopic properties with the microstructure of these eutectics.

2. Experimental

2.1. Samples fabrication

The precursor rods were obtained from the powder mixture of wollastonite (CS) and tricalcium phosphate (TPC) in the eutectic 80% $CaSiO_3$, 20% $Ca_3(PO_4)_2$ mol% composition. Furthermore, 0.5 wt% of Eu_2O_3 was added to the eutectic composite to obtain the doped samples. The resulting powders were isostatically pressed at 200 MPa for 2 minutes to obtain ceramic rods which were sintered at 1200°C for 10 hours.

Glass and glass-ceramic eutectic rods were obtained by the laser floating zone technique (LFZ), which has been described elsewhere in detail [7, 16]. This technique permits to control the solidification rate, providing high axial and radial thermal gradients in the liquid-solid interface, of a great importance in the microstructure domain, and opens up the possibility of fabricating eutectic glasses and glass-ceramics [7, 31–33]. The growth rates were varied in order to modify the crystalline character of the samples. Keeping the rod diameter constant at about 2.5 mm, the samples were grown in air at rates of 50 and 500 mm/h to yield glass-ceramic samples, and at 1000 mm/h to produce the glass sample. After growth they were annealed at 650°C for 5 h to relieve inner stresses.

The reactivity of the glass-ceramic samples was checked by an *in vitro* test carried out by immersing, for a three-month period, a glass-ceramic sample grown at 50 mm/h with diameter and length of 2.5 and 5 mm respectively, inside a polyethylene bottle with 100 ml of simulated body fluid (SBF) which was prepared according to the standard process [34]. The sample was kept at human body temperature of 37 °C by means of a Memmer Beschickung-loading-model 100-800 stove.

2.2. Characterization techniques

The microstructure, composition, and crystalline features of the phases present in the samples were determined by means of scanning electron microscopy (SEM), Energy-dispersive X-ray spectroscopy analysis (EDX), and Electron backscatter diffraction (EBSD), with a field emission JEOL JSM-7000F microscope.

Resonant time-resolved FLN spectra were performed by exciting the samples with a pulsed frequency doubled Nd:YAG pumped tunable dye laser of 9 ns pulsed width and 0.08 cm^{-1} linewidth and detected by an EGG&PAR Optical Multichannel Analyzer. The

#181528 - $15.00 USD Received 10 Dec 2012; revised 26 Feb 2013; accepted 1 Mar 2013; published 8 Mar 2013

measurements were carried out by keeping the samples temperature at 10 K in a closed cycle helium cryostat. For lifetime measurements, the fluorescence was analyzed with a 0.25 m Jobin-Ybon monochromator and the signal detected by a Hamamatsu R636 photomultiplier. Data were processed by a Tektronix oscilloscope.

3. Results and discussion

3.1 Compositional and microstructural characterization

In first instance, the chemical composition of the glass-ceramic samples was analyzed to verify that composition was around the eutectic point, 50.7 CaO + 31.0 SiO_2 + 18.3 P_2O_5 in wt%, and to check the amount of RE the samples were doped with. Table 1 shows the processing features of the glass-ceramic samples and the amount of oxides present in each one. As can be seen, the composition of the samples as well as the percentage of doping material were close to the nominal values. Traces of Mg, Fe, and Al impurities were also found.

Table 1. Compositional analysis of the W-TCP eutectic glass-ceramics in wt% together with the growth rate, V, the theoretical eutectic composition and the nominal doping composition of Eu_2O_3.

	V (mm/h)	***SiO_2***	***P_2O_5***	***CaO***	***Eu_2O_3***
Theoretical	-	31.00	18.30	50.70	0.50
Sample 1	50	30.28	18.95	50.77	0.63
Sample 2	500	30.40	18.95	50.65	0.70

In a previous work, the authors analyzed the microstructure of these eutectic glass-ceramics doped with Nd_2O_3 and found that they were composed of irregularly shaped fibers embedded in a matrix and aligned parallel to the growing direction [16]. The size and the number of phases depended on the growth rate, the rod diameter, and the amount of doping material present in the sample. In these glass-ceramics doped with Nd^{3+} ions, a growth rate increase led the system to a structural arrangement from three to two phases. Furthermore, regarding the crystalline nature of the phases, it was observed that, in the case of low-rate grown samples with three phases, the fibers had an apatite-like structure, which could be apatite, oxyapatite or hydroxyapatite, whereas the matrix was made up of two phases: one major phase, with Ca_2SiO_4 structure, and a minor phase which was amorphous. In the case of high-rate grown samples with two phases, the fibers also had an apatite-like structure, but in this case the matrix presented only one amorphous phase.

In order to analyse the influence of the rare earth nature on the microstructure of the glass-ceramic samples, a microstructural analysis was carried out by means of scanning electron microscopy (SEM). Regarding the morphology of the samples, the substitution of Nd_2O_3 by Eu_2O_3 did not produce any effect either on the arrangement or on the number of phases. As an example, Fig. 1 shows the longitudinal section of the glass-ceramic samples doped with 0.5 wt% of Eu_2O_3 grown at 50 mm/h (a) and 500 mm/h (b). The insets in the micrographs show the details of the microstructure in a cross-section view. The micrographs show how, as when doped with Nd_2O_3, the microstructure was made up of fibers with an irregular shape, aligned to the growing direction embedded in a matrix. In the same way, the number of phases present in the samples depended on the growth rate, so that at a low growth rate of 50 mm/h, the sample had three phases, i.e., the fibers (clear phase) and the matrix (dark and black phases), whereas at a high growth rate of 500 mm/h, there were only two phases in the sample, the fibers (clear phase) and matrix (dark phase).

#181528 - $15.00 USD Received 10 Dec 2012; revised 26 Feb 2013; accepted 1 Mar 2013; published 8 Mar 2013

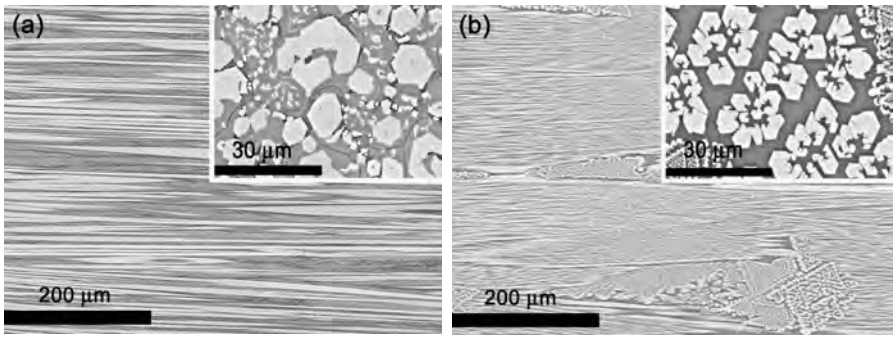

Fig. 1. Longitudinal-section of the glass-ceramic samples doped with 0.5 wt% of Eu_2O_3 grown at 50 mm/h (a) and 500 mm/h (b). The insets in the micrographs show the details of the microstructure in a cross-section view.

EDX analysis carried out to determine the composition of the phases in each sample showed a similar behaviour to the one observed for the Nd_2O_3 case. For samples with three phases, grown at low rate, the clear phase was rich in CaO and P_2O_5 with a low content of SiO_2. The dark phase was rich in SiO_2 and CaO with a very low content of P_2O_5, and in the black phase the amount of CaO and SiO_2 was high with a low content of P_2O_5. Regarding the amount of Eu_2O_3, it was found in the three phases, with a similar content in both the clear and dark phases, but with a much higher one in the black phase. In the case of samples with two phases, grown at high rate, the composition of the clear and dark phases was similar to the previous case. Table 2 shows the compositional analysis in wt% of samples grown at 50 mm/h and 500 mm/h doped with 0.5 wt% of Eu_2O_3.

Table 2. Compositional analysis in wt% of the phases present in the eutectic glass-ceramic samples grown at 50 and 500 mm/h.

	V (mm/h)	***SiO_2***	***P_2O_5***	***CaO***	***Eu_2O_3***
Clear Phase	50 mm/h	15.52	32.30	51.69	0.49
Dark Phase	50 mm/h	50.61	3.79	45.12	0.50
Black Phase	50 mm/h	55.93	10.58	31.64	1.85
Clear Phase	500 mm/h	16.20	31.68	51.63	0.48
Dark Phase	500 mm/h	48.75	9.62	40.81	0.82

With regards to the crystalline nature of the phases, EBSD analysis performed in the samples confirmed that the crystalline structures were the same as observed for the Nd_2O_3 case. Fibers (clear phase) were crystalline with an apatite-like structure in any case, whereas the dark phase turned from crystalline, with Ca_2SiO_4 structure, into amorphous as the growth rate increased. The black phase, which only appeared at low rate, was amorphous. Figure 2 shows the cross-section micrograph of a sample grown at 50 mm/h doped with 0.5 wt% of Eu_2O_3. The insets show the electron backscatter diffraction patterns corresponding to the oxyapatite structure found in the clear phase, (1), and to the dicalcium silicate found in the dark phase, (2).

#181528 - $15.00 USD Received 10 Dec 2012; revised 26 Feb 2013; accepted 1 Mar 2013; published 8 Mar 2013

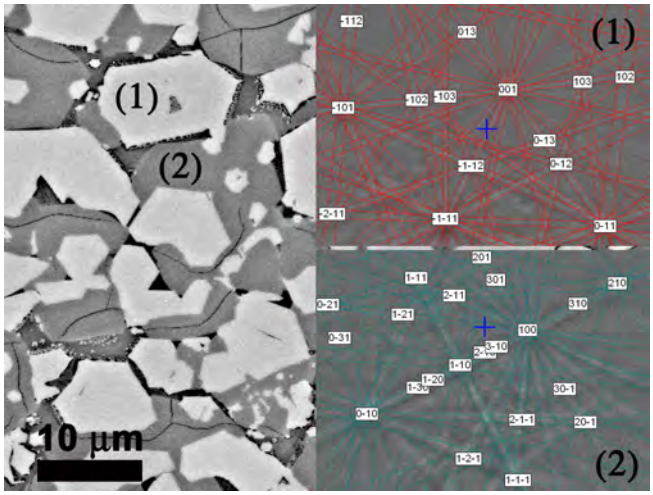

Fig. 2. Cross-section micrograph of a glass-ceramic sample doped with 0.5 wt% of Eu_2O_3 grown at 50 mm/h. The insets show the electron backscatter diffraction patterns corresponding to an oxyapatite structure found in the clear phase, (1), and to the dicalcium silicate found in the dark phase, (2).

On the other hand, the Ca_2SiO_4 structure observed in the glass-ceramic samples grown at low growth rate has shown an excellent *in vitro* bioactivity, since when soaked into SBF, a bonelike hydroxyapatite (CHA) layer is formed on the surface [35]. To ascertain the reactivity of the glass-ceramic sample grown at low rate, an *in vitro* preliminary test was carried out by soaking the sample grown at 50 mm/h into SBF for 3 months. Figure 3 shows the micrograph in a longitudinal-section view of the sample after the immersion period. It can be observed how the SBF has dissolved the two phases of the glass-ceramic matrix, the amorphous phase as well as the one with Ca_2SiO_4 structure, giving rise to a porous layer with a thickness of around 80 µm in which the fibers still remain in the sample. An EBSD analysis carried out in the sample confirmed that the apatite-like structure of the fibers was unaltered after the immersion period.

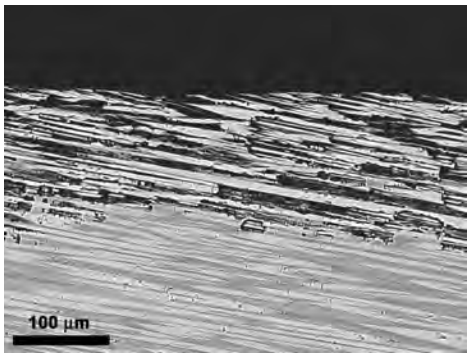

Fig. 3. Longitudinal -section micrograph of a glass-ceramic sample doped with 0.5 wt% of Eu_2O_3 grown at 50 mm/h after an immersion period of three months in simulated body fluid (SBF).

Therefore, we can conclude that the features of the LFZ growing technique permit to obtain glass-ceramic samples departing from a non-equilibrium state, resulting in microstructures not reported so far in this system that cannot be obtain by the conventional thermal treatments in furnace in which the substitution of the rare earth does not affect the microstructure of the glass-ceramic samples either in the morphology or in the crystalline structure.

#181528 - $15.00 USD Received 10 Dec 2012; revised 26 Feb 2013; accepted 1 Mar 2013; published 8 Mar 2013

3.2. Time-resolved fluorescence line-narrowing spectroscopy

As we have mentioned before, the optical properties of Eu^{3+} ions are highly sensitive to the local environment. Since the first excited state $^5D_0$ is non-degenerate, the structure observed in the fluorescence spectra is only determined by the terminal ground state splitting. Therefore, the $^5D_0 \rightarrow {}^7F_0$ transition clearly indicates there are different sites present in the host. Moreover, the $^5D_0 \rightarrow {}^7F_2$ transition is hypersensitive to the chemical surroundings and is symmetry dependent. Hence it is possible to distinguish between crystalline and glassy environments by means of time resolved fluorescence line narrowing spectroscopy.

Time-resolved line-narrowed fluorescence spectra of the $^5D_0 \rightarrow {}^7F_{0\text{-}2}$ transitions of Eu^{3+}-doped samples were obtained at 10 K by using different resonant excitation wavelengths into the $^7F_0 \rightarrow {}^5D_0$ transition with a time delay of 10 μs. Figure 4(a) shows the spectra corresponding to the $^5D_0 \rightarrow {}^7F_{0,1,2}$ transitions for the sample grown at 50 mm/h obtained at different pumping wavelengths along the $^7F_0 \rightarrow {}^5D_0$ absorption band. Depending on the excitation wavelength the emission spectra present different characteristics, mainly regarding the relative intensity of the transitions and the splitting. Under excitation between 572 and 576, the spectra show similar features to those observed in Eu^{3+}-doped apatites [27, 28]. In these spectra, the $^5D_0 \rightarrow {}^7F_0$ transition shows a strong intensity and the energy of the $^5D_0$ level is higher than in other Eu^{3+}-doped crystalline samples. Moreover, there is a significant splitting of the Stark components in which levels $^7F_1$ and $^7F_2$ overlap which indicates the presence of a highly asymmetric crystal field which produces mixing of the $^7F_1$ and $^7F_2$ states [27, 28]. In the apatite lattice Eu^{3+} can substitute the Ca^{2+} ions and therefore, as there are two inequivalent Ca sites, one ninefold coordinated with C_3 symmetry and the other sevenfold coordinated with C_s symmetry, the splitting of these transitions indicates that Eu^{3+} ions in the apatite-like crystalline phase occupy the low symmetry sites. The presence of slightly different sites can be explained by a slightly different arrangement of charge compensating ions and defects.

On the other hand, while tuning the excitation pulse at other wavelengths (578 nm) the spectra consist of a superposition of emissions corresponding to Eu^{3+} ions in different phases. The spectrum obtained by exciting at 579.1 nm is only observed in this sample and according to the EBSD analysis, corresponds to Eu^{3+} ions in dicalcium silicate crystalline phase. As in the case of the spectra corresponding to the apatite-like structure, three Stark levels for the $^5D_0 \rightarrow {}^7F_1$ transition and five levels in the hypersensitive $^5D_0 \rightarrow {}^7F_2$ transition are observed, meaning that Eu^{3+} ions are located in crystal sites with C_{2v} or lower symmetry.

In the case of the sample grown at 500 mm/h, where a crystalline and an amorphous phase are present, the spectra obtained under excitation between 572 and 576 nm show the same features than in the previous case corresponding to the emission from Eu^{3+} ions in the apatite crystalline phase. However, as excitation wavelength increases the spectra become similar to those obtained in the glass sample (see Fig. 4(b)).

As in the case of Nd^{3+} ions the dicalcium silicate phase appears only in the sample grown at low rate, in this case at 50 mm/h. This can be clearly observed in Fig. 5 which shows the emission spectra obtained under excitation at 579.1 nm for the GC samples grown at 50 mm/h and 500 mm/h and for the glass sample. As can be seen the emission spectrum of the sample grown at 500 mm/h is quite similar to the one obtained in the glass sample, which indicates that in this sample at this wavelength we are exciting Eu^{3+} ions in the amorphous phase. However, in the case of the glass-ceramic sample grown at 50 mm/h, the spectrum shows sharp lines according to Eu^{3+} in the dicalcium silicate crystalline phase. This is clear from the excitation spectra corresponding to the $^7F_0 \rightarrow {}^5D_0$ transition for the three samples (see Fig. 6). As can be seen, the excitation spectrum of the sample grown at 50 mm/h shows a band centered around 574 nm which corresponds to the apatite-like crystalline phase, together with a narrow peak around 579.1 nm, the excitation wavelength at which Eu^{3+} ions in the dicalcium silicate crystalline phase are excited. In the case of the sample grown at 500 mm/h,

#181528 - $15.00 USD Received 10 Dec 2012; revised 26 Feb 2013; accepted 1 Mar 2013; published 8 Mar 2013

the spectrum shows the band around 574 nm and a shoulder at the long wavelength side of the spectrum that corresponds to the Eu^{3+} ions in the amorphous phase.

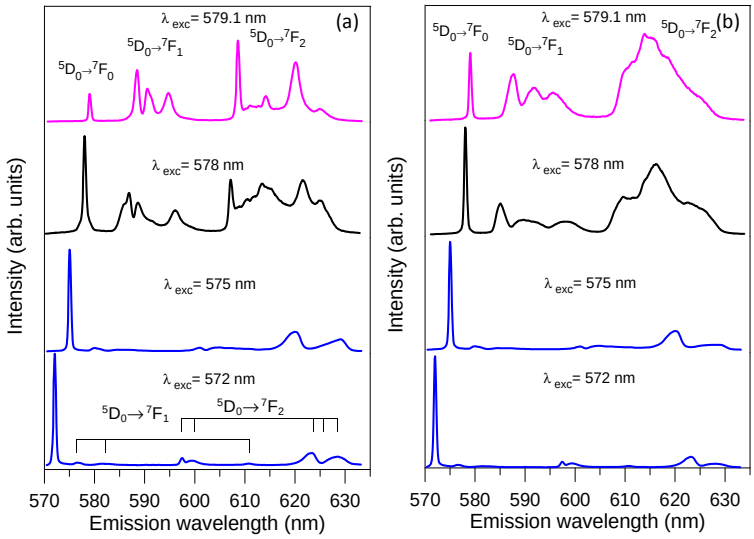

Fig. 4. $^5D_0 \rightarrow F_{0,\,1,\,2}$ emissions of Eu^{3+} in the sample grown at (a) 50 mm/h and (b) 500 mm/h obtained at different excitation wavelengths along the $^7F_0 \rightarrow ^5D_0$ absorption band. Data correspond to 10 K.

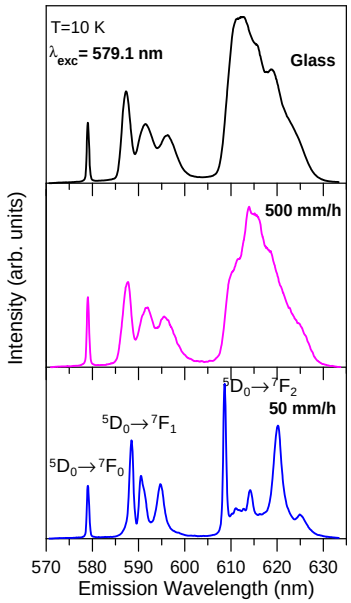

Fig. 5. $^5D_0 \rightarrow F_{0,\,1,\,2}$ emissions of Eu^{3+} for the glass-ceramic samples grown at 50 and 500 mm/h and for the glass sample obtained under excitation at 579.1 nm Data correspond to 10 K.

The presence of Eu^{3+} in the crystalline and amorphous phases is also confirmed by lifetime measurements of the $^5D_0$ level. As could be expected, if there are different sites for the Eu^{3+} ion, the lifetime of state $^5D_0$ should depend on the excitation wavelength. Thus, the lifetime of the $^5D_0$ state at different excitation wavelengths was measured and the luminescence at the highest intensity Stark component of the $^5D_0 \rightarrow ^7F_2$ transition collected.

#181528 - $15.00 USD Received 10 Dec 2012; revised 26 Feb 2013; accepted 1 Mar 2013; published 8 Mar 2013

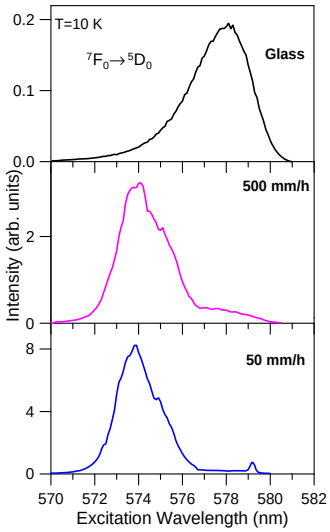

Fig. 6. Low temperature excitation spectra of the $^7F_0 \rightarrow {}^5D_0$ transition for the glass-ceramic samples grown at 50 and 500 mm/h and for the glass sample obtained by collecting the luminescence at the $^5D_0 \rightarrow {}^7F_2$ emission.

The temporal decays obtained under excitation at which the crystalline phases are selectively resolved can be described by a single exponential function. In the sample grown at 50 mm/h, the lifetime obtained under excitation at 579.1 nm which corresponds to Eu^{3+} in dicalcium silicate crystalline phase is around 3 ms whereas the lifetime corresponding to the apatite-like crystalline phase displays a variation from 0.448 to 0.661 as the excitation wavelength increases from 571.6 to 576 nm. At other wavelengths when Eu^{3+} ions are simultaneously excited in different phases, the decays are not single exponentials and the lifetimes change from 0.423 to 2.5 ms depending on the excitation and emission wavelengths. As an example Fig. 7 shows the experimental decays obtained by exciting at 574 and 579.1 nm and collecting the luminescence at the highest Stark component of the $^5D_0 \rightarrow {}^7F_2$ transition for the sample grown at 50 mm/h. In the case of the sample grown at 500 mm/h the decays obtained under excitation between 571 and 577 nm are single exponentials with lifetimes ranging between 0.47 and 0.77 ms. At longer wavelengths when Eu^{3+} ions in the apatite and amorphous phases are simultaneously excited, the decays are not single exponentials and lifetimes are longer. In the case of the glass sample the decays are single exponentials at all excitation wavelengths and the lifetime changes from 1.45 to 1.71 ms depending on the excitation wavelength. Therefore, as expected, lifetime measurements allow to identify the presence of Eu^{3+} ions in the different phases.

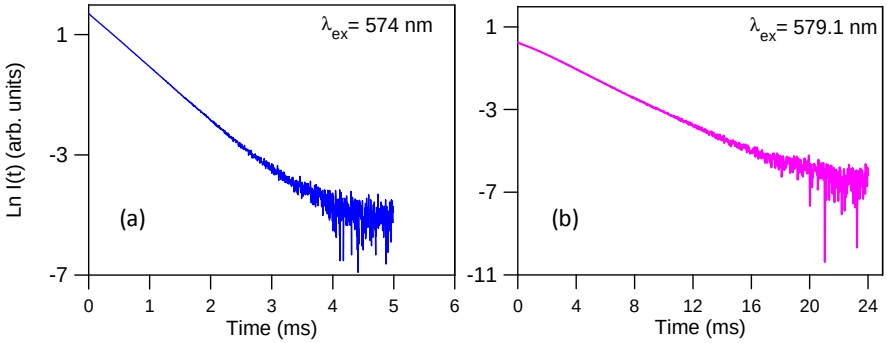

Fig. 7. Experimental decays of the $^5D_0$ level obtained under excitation at (a) 574 and (b) 579.1 nm and collecting the luminescence at the $^5D_0 \rightarrow {}^7F_2$ emission for the sample grown at 50 mm/h.

#181528 - $15.00 USD Received 10 Dec 2012; revised 26 Feb 2013; accepted 1 Mar 2013; published 8 Mar 2013

4. Conclusions

Eutectic glass and glass-ceramics samples of composition $0.8CaSiO_3$-$0.2Ca_3(PO_4)_2$ doped with 0.5 wt% of Eu_2O_3 were fabricated by the laser floating zone technique. This growing technique permits to obtain glass-ceramic samples starting from a non-equilibrium state and ending in not yet reported microstructures in this system that cannot be obtained by conventional thermal treatments in furnace. The microstructural analysis showed that the nature of the rare earth the samples were doped with, did not produce any effect either on the arrangement or on the number of phases, so that the growth rate is the key factor involved in the crystallization process and hence in the size and number of phases present in the glass-ceramic samples as well as in their crystalline features. In particular, the glassy character of the glass-ceramic samples increases with the growth rate in such a way that at high growth rates a glass sample can be obtained. For the glass-ceramic samples, the existence of three (two crystalline and one amorphous) or two phases (one crystalline and one amorphous), depending on the growth rate, has been shown. The crystalline phases correspond to Ca_2SiO_4 and apatite-like structures. The Ca_2SiO_4 structure observed in the glass-ceramic samples grown at low growth rate has shown high reactivity when soaked into simulated body fluid, so that the SBF dissolved this crystalline phase giving rise to a porous layer in which the apatite-like structure phase remains unaltered in the sample after the immersion period.

The results of fluorescence line narrowing experiments demonstrate the existence of three different local environments around the Eu^{3+} ions in these eutectic samples. The changes in the TRFLN emission spectra of Eu^{3+} ions related to the relative intensity and splitting of the Stark components of the $^5D_0 \rightarrow {}^7F_J$ transitions together with the different lifetimes values of the $^5D_0$ state depending on the excitation wavelengths allow to isolate the emission from Eu^{3+} ions in crystalline and amorphous environments and to correlate the spectroscopic properties with the microstructure of these eutectics. The emission from the two crystalline phases can be unambiguously identified from the emission and excitation spectra and lifetime measurements of the $^5D_0$ state of Eu^{3+} ions. These results show the potentialities of Eu^{3+}-doped eutectic glass-ceramics obtained from the LFZ technique as luminescence probes for in vitro applications based in their bioactive and luminescent properties.

Acknowledgments

This work was supported by the Spanish Government MEC under Projects No. MAT2009-14282-C02-02, FIS2011-27968, Consolider SAUUL CSD2007-00013, and Basque Country Government IT-331-07 and SAIOTEK S-PE12UN016. Daniel Sola thanks the JAE-DOC program and the Science and Technology Inter-Ministry commission of Spain and FEDER funds of the EC under project MAT2009-13979-C03-03 for the financial support of his contract.

#181528 - $15.00 USD Received 10 Dec 2012; revised 26 Feb 2013; accepted 1 Mar 2013; published 8 Mar 2013